Invited Paper

Consideration of solutions to the inverse scattering problem for biomedical applications

Michael V. Klibanov
University of North Charlotte, Department of Mathematics
Charlotte, North Carolina 28223

Semion Gutman
University of Oklahoma, Department of Mathematics
Norman, Oklahoma 73071

Randall L. Barbour and Jenghwa Chang
SUNY Health Science Center at Brooklyn, Department of Pathology
450 Clarkson Ave., Brooklyn, New York 11203

Joseph Malinsky
Sinai Medical School, Biomedical Department
One Gustave L. Place, New York, New York 10029-6517

Robert R. Alfano
City College of CUNY, Institute of Ultrafast Spectroscopy and Lasers
138th Street and Convent Avenue, New York, New York 10031

1.0 Introduction

For many situations in clinical medicine and other areas, knowledge of the interior structure and properties of materials is of great practical value. Imaging schemes which employed high energy sources, such as x-rays, have been the method of choice, in part, because of the high quality images that can be produced. While the undesirable biological effects of ionizing radiation have been known for several decades, it has only been within the past 15-20 years that alternative strategies that evaluate endogenous sources or exogeneous, but non-ionizing, sources have been made available. Endogenous sources include the electrical and magnetic fields produced as a result of synaptic propagation of the chemical signals generated in neuro-muscular tissues. Electroencephalographic (EEG) [1] and magnetoencephalographic (MEG) [2] imaging methods are based on measurement of these signals. Knowledge that body tissues contain ionic species that will conduct electrical current has led to the development of electrical impedance tomography (EIT) [3]. Within the electromagnetic spectrum, radio and microwave sources are also being explored for their suitability. When performed in the presence of a large external magnetic field, the former, has proven extremely successful in the form of magnetic resonance imaging [4,5]. The observation that mechanical energy will differentially propagate in tissue has led to acoustic imaging methods in the form of ultrasound imaging and more recently as acoustic tomography [6]. More recently, the search for identifying alternative sources for imaging studies has been extended into the near infrared range [7-9]. At these frequencies it is known that whereas light is intensely scattered by tissue, NIR photons will penetrate deeply, allowing measurements through the head of a neonate or an adult female breast [10]. The great sensitivity of optical measurements and the known relationship between tissue function and the oxygen-dependent spectral properties of hemoglobin and other heme proteins has underscored interest in this area.

With the exception of MRI, the quality of images produced using these alternative sources has been significantly poorer than that achieved using high energy sources. Frequently, though, the informational value of the resultant images is not strictly dependent on an accurate mapping of anatomical structures. For example, the acquisition of signals in real-time has proven especially valuable for sonography and for EEG, MEG, and EIT imaging and the closely associated electrocardiographic imaging method. Further, the ability to directly relate the measured response to well defined physiological events has also served to extend the usefulness of these methods.

8194-1114-0/93/$6.00

While the precise reasons accounting for the image quality obtained vary with the different methods, a common aspect of all is the considerable uncertainty which can exists as to the spatial origin of, in the case of endogenous sources, or path taken by, in the case of penetrating energy, the detected signal. When electromagnetic or acoustic sources are employed, this uncertainty is a result scattering of the penetrating energy due to localized differences in permittivity that is produced as a consequence of the physiochemical and structural heterogeneity of tissues. The theoretical framework for evaluating such measurements is described by the wave equation and is the basis for Diffraction Tomography (DT) [11]. As general rule, problems whose detector responses are dominated by scattering are typically ill-posed as multiple descriptions of the underlying medium may be consistent with the measured data. Invariably, another attribute of these types of problems is the considerable computing effort required to produce the resultant image, especially if a map in 3-dimensions rather than 2-D is required. In practice, the cost and time constraints imposed by the computing effort dominate and is the key element in defining the application range that a particular measurement-algorithm scheme may have. Theoretically sound strategies that rely on brute force computations frequently have little practical value.

The need to effectively balance the measurement-algorithm scheme with acceptable computing times has led to the development of a variety of image recovery strategies. The Born and Rytov approximations, for example, introduce the assumption that the intensity of scattered signal is small relative to the incident field thereby linearizing the problem [11]. Recent studies, however, have demonstrated that this approximation cannot provide sufficient accuracy in the resultant images [12,13]. Other schemes provide a nonlinear treatment of the data and obtain convergence by minimizing a specified cost functional. These methods differ in their starting points. Newton-type methods usually consider a homogeneous background and update Born-Rytov approximations in an iterative process [12, 13]. Solutions of non-Newton methods are not dependent on employing a "good" initial first guess as to the properties of the medium [14-16].

In general, efforts to solve inverse scattering problems (ISP), especially in the 3-D case, are difficult because of the following factors: i) Ill-conditionedness; small random fluctuations in the data cause large variations in the solution; ii) inherent nonlinearity of measured data with respect to unknown coefficients; iii) very large scale computations because unknown coefficients essentially depend on three, rather than two spatial variables. Attempts to address these concerns invariably involve tradeoffs. For example, all of the approaches described above require minimization of some type of functional. In doing this one faces at least one of the following procedures which are rather time consuming, even in the 2-D case. i) Solution of a boundary value problem for Helmholtz-like equation; ii) computation of a large number of 2-D, or 3-D integrals on each iteration step; iii) implementation of regularization techniques that require computing multiple solutions of (i) and (ii) in order to choose a proper value of the regularization parameter; (iv) properties of minimizing cost functionals are usually not investigated theoretically, which, in principle, can lead to the presence of multiple local minimums that may further add to the computational burden for search of the global minimum, especially in the case of a large number of unknowns [17]. Clearly, the correct solution requires determining the global minimum. Overall, whereas various techniques have been successfully developed to address the issue of ill-posedness, the practical applicability of these becomes increasingly problematic as the size of the computing problem grows (i.e. 3-D case) and alternative numerical strategies must be sought.

Recently, a new approach for solving ISPs has been described by some of the co-authors [18-22]. We call this the Regularized Quasi-Reversibility approach (RQR). The *core* of the RQR scheme consists of working directly with partial differential equations, rather than with associated integral equations (e.g. as for instance, Lippman-Schwinger integral equation). Computational efficiency is accomplished by using explicit precalculation of all needed integrals, a priori choice of the number of Fourier coefficients of the unknown function as a regularization parameter, and construction of quasi-solutions of needed boundary value problems rather than construction of actual solutions. Alternatively, similar efficiencies are obtained through construction of a globally convex minimizing cost functional that has the attractive feature of a single minimum. Examination of the method indicates that it is computationally efficient and results presented here, and elsewhere [18,19,22] for the Helmholtz and time-dependent wave equations confirm this. For example accurate solutions in the 2-D case have been obtained for inverse problems containing 441 unknowns (solved iteratively) in less than one minute of CPU time using a Y/MP-CRAY. In fact recent preliminary results (not shown) have indicated that 3-D problems involving 3,000-4,000 unknowns can be computed in less than 30 minutes.

In this report we describe two versions of the RQR approach and present results demonstrating the accuracy and stability of the solutions, in the 2-D case, based on evaluation of time-independent as well as time-dependent data. We also provide a discussion which considers the potential applicability of these methods to evaluate time-resolved optical measurements from dense scattering media obtained using ultrafast laser sources operating at NIR frequencies. The compatibility of this approach with solution of the ISP based on the transport equation is also described.

2.0 Methods

I. *RQR Method for an ISP for Helmholtz-like Equation*

Statement of Forward Problem

Let $\Omega \subset R^3$ be a bounded domain in 3-D space with an unknown function $\varepsilon(\vec{x}) = \bar{\varepsilon}\left(1+\tilde{\varepsilon}(\vec{x})\right)$, where $\bar{\varepsilon} = \text{constant}$ is the averaged ε of the background and $\tilde{\varepsilon} = \left(\varepsilon(\vec{x}) - \bar{\varepsilon}\right)/\bar{\varepsilon}$ is the relative fluctuation of ε. In electrodynamics $\varepsilon(\vec{x})$ can be treated as the dielectric permittivity, in acoustics $\varepsilon(\vec{x})$ represents the speed of sound. We assume that $\Omega \subset S$, where S is a sphere of radius $\pi/2$ with the center at the origin. Let S^2 be the surface of the unit sphere in R^3. If $\vec{\nu} \in S^2$, then $e^{ik\langle \vec{x}, \vec{\nu} \rangle}$ is the scalar incident planar wave propagating in the direction of the vector $\vec{\nu}$. Here $\langle \cdot, \cdot \rangle$ is the inner product in R^3. Let $u(\vec{x}, \vec{\nu})$ be the solution of the forward scattering problem where,

$$\Delta u + k^2\left(1+\tilde{\varepsilon}(\vec{x})\right)u = 0, \tag{1.1}$$

and

$$u(\vec{x}, \vec{\nu}) = e^{ik\langle \vec{x}, \vec{\nu} \rangle} + \tilde{u}(\vec{x}, \vec{\nu}), \tag{1.2}$$

including Sommerfeld radiation conditions, and k is the wave number.

The ISP Statement

Let ∂S be the boundary of the sphere S, and k = constant > 0. The objective here is to determine the function $\tilde{\varepsilon}(\vec{x})$ in eqs. (1.1, 1.2), assuming $\tilde{\varepsilon}(\vec{x}) = 0$ outside Ω and that one measures the function $u(\vec{x}, \vec{\nu})$ on ∂S for all $\vec{\nu} \in S^2$. Hence, the following function is given

$$u\big|_{\partial S} = \phi(\vec{x}, \vec{\nu}), \qquad \forall\, \vec{\nu} \in S^2 \tag{1.3}$$

which describes the measured data.

Our measurement scheme is plotted in Figure 1. Note that equation (1.1) is dimensionless as are the variables $\vec{x}$, k.. For any real application, equation (1.1) can be rescaled by the formulas

$$\vec{x} = \vec{x}'\frac{\pi}{d}, \qquad k = \frac{2d}{\lambda}, \tag{1.4}$$

where d is the size of the target medium, x' is the "real" position vector and λ is the wave length of the incident field.

For many of the applications in DT, the function $u(\vec{x}, \vec{\nu})$ amounts to measuring the phase and amplitude of the emerging signal. In the next section we show how the *ISP* in (1.1-1.3) can be evaluated without direct phase measurements.

As described in the Discussion, we consider this, in part, in recognition of the practical difficulty of obtaining phase measurements using optical sources with highly scattering media.

Solutions to *ISP* eqs. (1.1-1.3)

Let G be a cube, bounded by ∂G, where G = $\{-\pi < x_1, x_2, x_3 < \pi\}$. Hence $S \subset G$. Using the function $\phi(\vec{x},\vec{v})$, described in equation (1.3), we can obtain a function $F(\vec{x},\vec{v})$ such that $F(\vec{x},\vec{v}) = 0$ inside S and

$$u\big|_{\partial G} = F(\vec{x},\vec{v})\big|_{\partial G}, \qquad \frac{\partial u}{\partial n}\Big|_{\partial G} = \frac{\partial \vec{F}}{\partial n}(\vec{x},\vec{v})\Big|_{\partial G}, \tag{1.5}$$

where $\vec{n}$ is the outward normal vector on ∂G. Lets introduce a function $V(\vec{x},\vec{v})$, where $V(\vec{x},\vec{v}) = u(\vec{x},\vec{v}) - F(\vec{x},\vec{v})$. Based on equations (1.1) through (1.3) the following may be deduced.

$$\Delta V + k^2\left(1+\tilde{\varepsilon}(\vec{x})\right)V + k^2\tilde{\varepsilon}(\vec{x})F = -\left(\Delta F + k^2 F\right), \tag{1.6}$$

$$\text{and} \qquad V\big|_{\partial G} = \frac{\partial V}{\partial n}\Big|_{\partial G} = 0.$$

The objective here is to solve the system in (1.6) in order to determine both functions $\tilde{\varepsilon}(\vec{x})$ and $V(\vec{x},\vec{v})$. Let N be a positive integer such that $N \le k\frac{2}{\sqrt{3}}$ in the 3-D case and $N \le \sqrt{2}k$ in the 2-D case. We seek the function $\tilde{\varepsilon}(\vec{x})$ as the following Fourier series

$$\tilde{\varepsilon}(\vec{x}) = \sum_{|\vec{m}|\le N} A_m e^{i\langle \vec{x},\vec{m}\rangle} \tag{1.7}$$

where $\vec{m} = (m_1, m_2, m_3)$ are vectors with integer coordinates and A_m are Fourier coefficients of the function $\tilde{\varepsilon}(\vec{x})$. The essence of our numerical method consists of an iterative search of coefficients A_m and Fourier coefficients of the function $V(\vec{x},\vec{v})$ obtained using the quasi-Newton method. On the first iteration this method inverts the Born approximation as is obtained in other approaches in DT [11]. In subsequent iterations our method performs the steps described below. We have rigorously proven previously that our method converges [19].

(i) Let N be a positive integer such that $\sqrt{3}N \le 2k$. Let P be the set of points $z \in R^3$ such that the coordinates (z_1, z_2, z_3) of z be integers and satisfy $|z_i| \le N, i = 1,2,3$. Also, M and γ are positive numbers such that $\gamma^2 + 2k^2$ is a noninteger; we usually assign γ = 0.3.

(ii) For each z∈P find a unit vector $\vec{v}_z \in S^2$ such that $2k(\vec{v}_z,\vec{z}) = |\vec{z}|^2$.

(iii) Define initial values of $\tilde{\varepsilon}, V$ as $\tilde{\varepsilon}_0(\vec{x}) = 0$, and $V_0(\vec{x},\vec{v}_z) = u_0(\vec{x},\vec{v}_z) - \Phi(\vec{x},\vec{v}_z)$, where $u_0(\vec{x},\vec{v}) = e^{ik\langle \vec{x},\vec{v}\rangle}$.

(iv) Construct the sequence $\{\tilde{\varepsilon}_n(\vec{x}), V_n(\vec{x},\vec{v}_z)\}$ (where z∈P) iteratively as follows.

a) For every z∈P, let

$$f_n(\vec{x},\vec{v}_n) = -k^2\tilde{\varepsilon}_{n-1}u_0(\vec{x},\vec{v}_z) - k^2\tilde{\varepsilon}_{n-1}\left(V_{n-1}(\vec{x},\vec{v}_z) + \Phi(\vec{x},\vec{v}_z)\right) - \left(\Delta\Phi(\vec{x},\vec{v}_z) + k^2\Phi(\vec{x},\vec{v}_z)\right).$$

b) For z∈P, compute the Fourier coefficients of $\tilde{\varepsilon}_n$ as

$$\tilde{\varepsilon}_n{}^z = \frac{1}{k^2}\int_{\Omega_1} f(\vec{x},\vec{v}_z)e^{i\langle \vec{x},\vec{z}-k\vec{v}_z\rangle}d\vec{x}.$$

c) Let

$$\tilde{\varepsilon}_n(\vec{x}) = \frac{1}{(2\pi)^3}\sum_{z\in P}\tilde{\varepsilon}_n{}^z e^{-i\langle \vec{x},\vec{z}\rangle}.$$

d) For every $\vec{Y}=(y_1,y_2,y_3)\in P$, compute the Fourier coefficients of V_n as

$$W^Y{}_{n,Z} = \frac{1}{p(k,\vec{Y},\vec{v}_z)}\left[-k^2\int_G \tilde{\varepsilon}_n e^{-\gamma\langle \vec{x},\vec{v}_z\rangle + i\langle \vec{x},\vec{Y}\rangle}d\vec{x} + \int_G f_n \exp[-(\gamma + ik\langle \vec{x},\vec{v}_z\rangle + i\langle \vec{x},\vec{Y}\rangle)]d\vec{x}\right], \text{ where}$$

$$p(k,\vec{Y},\vec{v}_z) = 2k\langle \vec{v}_z,\vec{Y}\rangle - 2i\gamma\langle \vec{v}_z,\vec{Y}\rangle - |\vec{Y}|^2 + 2i\gamma k + \gamma^2.$$

e) Let $V_n(\vec{x},\vec{v}_z) = \frac{1}{(2\pi)^3}e^{(\gamma+ik)\langle \vec{x},\vec{v}_z\rangle}\sum_{Y\in P} W^Y{}_{n,z}e^{-i\langle \vec{x},\vec{Y}\rangle}$.

It is important to note that all integrals here can be either *precalculated* explicitly or very rapidly using the Fast Fourier Transform. We also note that function $V_n(\vec{x},\vec{v}_z)$ is a quasi-solution of the boundary value problem: $\Delta V_n + k^2 V_n = -f_n$, $V_n\big|_{\partial G} = \frac{\partial V_n}{\partial n}\big|_{\partial G} = 0$. But V_n does *not* necessarily satisfies these boundary conditions. We can rigorously prove, however, that $\lim_{n\to\infty}\sum_{Z\in P}\left|\tilde{\varepsilon}^z{}_n - A_z\right|^2 = 0$.

We have carried out a total of 30 numerical experiments in the 2-D case. This method is very fast, requiring approximately only one minute for twelve iterations at N=10 using a Y/MP-CRAY. Thus, this involves computing, iteratively, 441 unknown Fourier coefficients of the function $V(\vec{x},\vec{v}_z)$ for each of the 441 directions, $\vec{v}_z$, of the incident plane waves to obtain the values of 441 unknown Fourier coefficients of function $\tilde{\varepsilon}$, thereby requiring computation of a total of $(441^2 + 441)$, 194,922 unknowns.

Computation of Relative Error:

Let $\tilde{\varepsilon}_t$ be the tested function $\tilde{\varepsilon}(\vec{x})$ which is represented by the Fourier series described in equation (1.7). The computed values of $\tilde{\varepsilon}$, indicated by $\tilde{\varepsilon}_c$,, obtained by solving the inverse problem, can then be compared to $\tilde{\varepsilon}_t$. The calculated relative error is $\frac{\|\tilde{\varepsilon}_t - \tilde{\varepsilon}_c\|}{\|\tilde{\varepsilon}_c\|}$, (1.8)

where $\|\cdot\|$ is the L_2-norm given by $\|\tilde{\varepsilon}\| = \left[\sum_{|m|\le N} |A_m|^2\right]^{\frac{1}{2}}$. The method described here is restricted to considering values of k between 5 and 15 and $k|\tilde{\varepsilon}|A<1$, where A is the area of the domain where $\tilde{\varepsilon} \neq 0$.

II. *RQR Method for Time Dependent Wave Equation*

Consider an impluse function directed to a target medium. This pulse can be described as $\delta\left(t-\frac{z}{V_g}\right)\delta(x,y)e^{i\omega\left(t-\frac{z}{V_g}\right)}$, where ω is the frequency of the carrier, δ is the delta function and V_g is the group velocity of the wave packet. The pulse enters the medium at t = 0 at the point (0,0,0). Let $\vec{E} = (E_1, E_2, E_3)$ be the vector of the electric field and $\vec{x} = (x,y,z)$. The initial values of the three components of the vector E are defined as

$$E_1(\vec{x},0) = \delta\left(\frac{z}{V_g}\right)\delta(x,y), \tag{2.1a}$$

$$\frac{\partial E_1}{\partial t}(\vec{x},0) = 0, \tag{2.1b}$$

$$E_2(\vec{x},0) = \frac{\partial E_2}{\partial t}(\vec{x},0) = E_3(\vec{x},0) = \frac{\partial E_3}{\partial t}(\vec{x},0) = 0 \tag{2.1c}$$

Our first and third conditions of (2.1) mean that we are following the center of the wave envelope, the second condition is a mathematical statement of the assumption that we have no energy flux in the medium until the wave enters it. Let c be the speed of light in a vacuum and $\varepsilon(\vec{x}) = \bar{\varepsilon}(1+\tilde{\varepsilon}(\vec{x}))$ be the dielectric function of the medium. The following equation follows immediately from the Maxwell system:

$$\frac{\varepsilon}{c^2}\frac{\partial^2 \vec{E}}{\partial t^2} = \Delta\vec{E} + \nabla\left[\vec{E}\nabla(\ln\varepsilon)\right] \tag{2.2}$$

where $\Delta = \nabla^2$ is the Laplace operator. We assume that we are dealing with soft biological tissues, where $\tilde{\varepsilon}(\vec{x})$ varies slowly compared to variations of the electric field. Thus it is appropriate to neglect the second term in the right hand side of (2.2). It follows from eqs. (2.1), (2.2) that $E_2 \equiv E_3 \equiv 0$ and function $E_1 = u$ is the solution of the following initial value Cauchy problem $\frac{\varepsilon}{c^2}u_{tt} = \Delta u$, $u|_{t=0} = \delta(\vec{x}-\vec{x}_0)$, $u_t|_{t=0} = 0$, where $\vec{x}_0$ is the point at which the pulse enters the medium, not necessarily the origin. The same equation, with the same initial data, is also valid for the H_2 component of the magnetic field $\vec{H}$ and $H_1 \equiv H_3 \equiv 0$. Since the functions E_1 and H_2 satisfy the same wave equation with the same initial data then $E_1(\vec{x},t) \equiv H_2(\vec{x},t) \equiv u(\vec{x},t)$ for t > 0.

We assume that our medium is located inside a sphere S' and we measure the intensity of the emerging energy, $I(\vec{x},t)$ on the surface of the sphere S' as a function of time. The ISP consists of determining $\tilde{\varepsilon}(\vec{x})$ inside S' using these

measurements. First, we rescale this problem by introducing new variables $\vec{y} = \vec{x}\frac{\pi}{d}$, $\tau = \frac{c\pi}{\bar{\varepsilon}d}t$, where d is the size of the medium, see also (1.4). After rescaling we can assume that our dimensionless medium is located inside of the sphere S described previously. We obtain

$$\left(1+\tilde{\varepsilon}(\vec{y})\right)u_{\tau\tau} = \Delta u$$

$$\text{and} \quad u\big|_{\tau=0} = \left(\frac{\pi}{d}\right)^3 \delta(\vec{y}-\vec{y}_0), \text{ and } u_\tau\big|_{\tau=0} = 0, \tag{2.3}$$

where d is already dimensionless as a result of considering the delta function. We ignore absorption, so that $\tilde{\varepsilon}$ is a real valued function as does function u. From the Pointing vector consideration [23,24] we obtain on the surface of the sphere S

$$u^2(\vec{y},\tau)\big|_{\vec{y}\in\partial S} = I(\vec{y},\tau). \tag{2.4}$$

Eqs. 2.3, 2.4 is the statement of the ISP. But for our method we need to know the function $u(\vec{y},\tau)$ itself on S, not its square. By (2.4) $u = \pm\sqrt{I(\vec{y},\tau)}$ on ∂S. It should be emphasized that whereas the function u can have both positive and negative values for any wave phenomenon, when considering a wave packet, such as would be produced by an ultrafast laser source, the value of u is strictly positive following arrival of the first photons. This follows because $I(\vec{y},\tau) \neq 0$ after the first portion of photons enter the detector and experimental data obtained from ultrafast laser pulses justifies this assertion [25]. Hence, $u(\vec{y},\tau)$ is also $\neq 0$ for $\vec{y}\in\partial S$ under these conditions. If $\tilde{\varepsilon} = 0$, then $\int_0^t d\tau \int_0^\tau u(\vec{y},s)ds \geq 0$ [26]. Thus we take $u = \sqrt{I(\vec{y},\tau)}$. We can uniquely solve the following boundary value problem: $u_{\tau\tau} = \Delta u$, for $\vec{y}\in R^3 \setminus S, \tau > 0$,

$$u\big|_{\tau=0} = \left(\frac{\pi}{d}\right)^3 \delta(\vec{y}-\vec{y}_0), \quad \text{and } u_\tau\big|_{\tau=0} = 0, \text{ and } u\big|_{\vec{y}\in\partial S} = \sqrt{I(\vec{y},\tau)}.$$

Solution of the above yields $$u\big|_{\vec{y}\in\partial S} = \sqrt{I(\vec{y},\tau)}, \qquad \frac{\partial u}{\partial n}\Big|_{\vec{y}\in\partial S} = q(\vec{y},\tau,), \tag{2.5}$$

where the function $q(\vec{y},\tau,)$ is known. Thus eqs. (2.3), (2.5) represent a complete description of the ISP.

Solutions to ISP:

One approach for solving the ISP eqs. (2.3), (2.5) involves considering the Fourier transform of the function

$$V = \int_0^\infty e^{ik\tau}u(\vec{y},\tau)d\tau. \text{ Then } \Delta V + k^2\left(1+\tilde{\varepsilon}(\vec{y})\right)V + \left(\frac{\pi}{d}\right)^3 \delta(\vec{y}-\vec{y}_0) = 0 \tag{2.6}$$

$$V\big|_{\partial S} = g_1(\vec{y},k), \quad \frac{\partial V}{\partial n}\Big|_{\partial S} = g_2(\vec{y},k) \tag{2.7}$$

where g_1 and g_2 are Fourier transforms of functions $\sqrt{I(\vec{y},\tau)}$ and $q(\vec{y},\tau)$ respectively. Now assume that the source $\vec{y}_0$ is sufficiently far from the medium. In doing this we should assume that the wave packet satisfies the wave equation even before reaching the medium (see eq. (2.1)). This is reasonable because the pulse shape is nearly Gaussian and in the limit is equivalent to an impulse function. As described in reference [23], such functions are known to approximately satisfy the

wave equation. Thus let $\vec{y}_0$ be far away from the medium. We denote $\vec{\nu}=\frac{\vec{y}_0}{|\vec{y}_0|}$ and introduce the function $w=4\pi\left(\frac{d}{\pi}\right)^3 e^{ik|\vec{y}_0|}|\vec{y}_0|V^*$, where * is the complex conjugation. It follows from the above that we can recast w as the solution of the subsequent equations, which have the same form as eqs. (1.1), (1.2)

$$\Delta w+k^2\left(1+\tilde{\varepsilon}(\vec{y})\right)w=0,\ w=e^{ik\langle\vec{y},\vec{\nu}\rangle}+\tilde{w}, \tag{2.8}$$

where $\tilde{w}$ satisfies Sommerfeld radiation conditions. In fact the transform from (2.6) to (2.8) is well known [23].

The functions $w|_{\partial S}$, and $\frac{\partial w}{\partial n}|_{\partial S}$ can be derived from functions g_1, g_2 defined in eq. (2.7). Therefore now we can apply the method outlined in section I of Methods. We want to emphasize that in (2.5) we use only intensity measurements. On the other hand, we reduced the ISP, eqs. (2.3), (2.5) to the ISP (1.1) through (1.3). We obtained "phase" measurements by transform only.

Another way of treating the ISP of (2.3), (2.5) lies in working directly with the time resolved wave equation (2.3) without the need of any transform. In doing this we consider a single source location, rather than many sources as implied in (1.1) - (1.3). Uniqueness theorems for the "single source" case can be found in [26, 27]. Because the principal part of the differential operator in (2.3) is non-constant, the ISP (2.3), (2.5) is rather difficult to investigate. Consequently we have developed a quasi-Newton method for a similar ISP for a model equation.

Let function $a(\vec{y})=0$ outside of the sphere S and function $V(\vec{y},\tau)$ be the solution of the following Cauchy problem

$$V_{\tau\tau}=\Delta V+a(\vec{y})V,\ \text{given the initial data } V|_{\tau=0}=0,\ \text{and } V_\tau|_{\tau=0}=\delta(\vec{y}-\vec{y}_0). \tag{2.9}$$

The ISP requires determination of the potential $a(\vec{y})$ by functions

$$V|_{\partial S}=f_1(\vec{y},\tau),\quad \frac{\partial V}{\partial n}|_{\partial S}=f_2(\vec{y},\tau) \tag{2.10}$$

We note that by considering the function $V_1=\int_0^\tau V(\vec{y},s)ds$, we obtain the same initial data as in (2.3). Below we describe the quasi-Newton method for the ISP (2.9), (2.10).

Denote $a_0(\vec{y})=0$, and $V_0(\vec{y},\tau)=\frac{\delta(\tau-|\vec{y}-\vec{y}_0|)}{4\pi|\vec{y}-\vec{y}_0|}$. Thus function V_0 is the solution of the Cauchy problem in the case $a=a_0=0$, for a non-scattering medium.

Iteration number m ≥ 1. Assume that functions a_{m-1}, V_{m-1} have been already found. We solve the following boundary value problem. $(W_m)_{\tau\tau}-\Delta W_m=[\Delta V_{m-1}-(V_{m-1})_{\tau\tau}+a_{m-1}V_{m-1}]$

$$W_m|_s=p_{m-1}(\vec{x},\tau),\quad \frac{\partial W_m}{\partial\vec{n}}|_{\partial S}=q_{m-1}(\vec{x},\tau) \tag{2.11}$$

where $p_{m-1} = \begin{cases} f_1, \text{ for m} = 1 \\ 0, \text{ otherwise} \end{cases}$, $q_{m-1} = \begin{cases} f_2, \text{ for m} = 1 \\ 0, \text{ otherwise} \end{cases}$. Then we take functions

$$a_m(\vec{x}) = a_{m-1}(\vec{x}) + 8\pi\left(\frac{\partial W_m}{\partial|\vec{x}|} + \frac{\partial W_m}{\partial\tau}\right)(\vec{x}, \tau = |\vec{x}|) \quad \text{and} \quad V_m(\vec{x},\tau) = V_{m-1}(\vec{x},\tau) + W_m(\vec{x},\tau).$$

The steps in the boundary value problem given in eq. (2.11) are the *core* of our quasi-Newton method. The problem in eq. (2.11) is an ill-conditioned, non-traditional problem [26]. In fact, similar problems for the Laplace equation $\Delta W = 0$ arise in electrocardiography where the objective is to find the electric potential on the surface of the heart from knowledge of the potential on the surface of the chest [28, 29]. In a more general form, the problem in eq. (2.11) can be formulated as: Find function $u(\vec{x},t)$ satisfying the following conditions

$$u_{tt} - \Delta u = f(\vec{x},t) \text{ for } \vec{x} \in S, t \in (0,T),$$

$$u\big|_{\partial S} = \varphi_1(\vec{x},t), \quad \frac{\partial u}{\partial n}\Big|_{\partial S} = \varphi_2(\vec{x},t), \tag{2.12}$$

where T = constant > diam. (S). We call this the **field extension** problem. Here the objective is to compute the time-resolved signal inside the medium about a designated volume of interest. In [22] we have solved problem (2.12) numerically in the 2-D case. For convenience we have replaced the sphere, S, by the rectangle $D = \{x_1, x_2 : 0 < x_1, x_2 < 1\}$, and have chosen $\varphi_1 = \varphi_2 = 0$, see Fig 2. The more general case can be handled similarly. Let $Q_T = D \times [0,T]$, and δ be a small positive regularization parameter and introduce the differential operator $Lu = u_{tt} - \Delta u$. By our method we seek the

function u^δ which satisfies the integral identity $\int_{Q_T}\left(\frac{1}{\delta}Lu^\delta Lh + u^\delta{}_{tt}h_{tt} + \sum_{i=1}^{2} u^\delta{}_{x_i x_i}h_{x_i x_i} + u^\delta h\right)dxdt = \frac{1}{\delta}\int_{Q_T} fLh,$ (2.13)

for all twice differentiable functions h with $u^\delta, h, \frac{\partial u^\delta}{\partial n}$ and $\frac{\partial h}{\partial n}$ vanishing on $\partial D \times [0,T]$. We have rigorously proven that

$\lim_{\delta \to 0^+} \left\| u^\delta - w \right\|_{L_2(D_T)} = 0.$

3.0 Results

ISP for the Heimholtz Equation

Figure 3 shows a plot of the function $\mathrm{Re}\left[u(\vec{x},\vec{v})e^{-ik\langle\vec{x},\vec{v}\rangle}\right]$ and represents a computation of the scattered field from a

cylinder in which $\tilde{\varepsilon}(\vec{x}) = \tilde{\varepsilon}(r) = \begin{cases} 0.03, \text{ for } r < \frac{\pi}{2} \\ 0, \text{ otherwise} \end{cases}$ where $r = \sqrt{x^2{}_1 + x^2{}_2}$, $\vec{v} = (1,0)$, and $k = 5.3$. This data is representative of the type of scattering encountered in the forward problem whose solution was used as input for the inverse problem for media having cylindrical geometry. Note that the scattered field is mostly limited to the forward hemisphere. Since the forward problem described by eqs. (1.1) and (1.2) does not allow for explicit solution for any case other than a medium having cylindrical geometry, we have simulated values of u for the inverse problem (1.1, 1.3) for media having non-cylindrical geometry as follows. We consider solution of the boundary value problem $\Delta w + k^2\left(1 + \tilde{\varepsilon}(\vec{x})\right)w = 0$, where

$\frac{\partial w}{\partial n}\big|_{\partial G} = \frac{\partial}{\partial n}\left(e^{ik\langle \vec{x},\vec{v}\rangle}\right)\big|_{\partial G}$. For the real variable y, let $\xi(y) = \begin{cases} 1, \text{ for} |y| < \frac{\pi}{2} \\ \sin^4 y, \text{ for } |y| \geq \frac{\pi}{2} \end{cases}$ and introduce

function $\alpha(x_1, x_2) = 1 - \xi(x_1)\xi(x_2)$. Let $F(\vec{x},\vec{v}) = w\alpha$, then $F(\vec{x},\vec{v}) = 0$ for $|x_1|, |x_2| < \frac{\pi}{2}$, and

$\frac{\partial w}{\partial n}\big|_{\partial G} = \frac{\partial}{\partial n}\left[F(\vec{x},\vec{v})\right]$, and $w\big|_{\partial G} = F(\vec{x},\vec{v})$. Then we let $V = w - F$ and obtain (1.6). For these computations and results presented subsequently (tests #1-6), we have employed a source-detector configuration illustrated in Figure 1, which shows that for each incident planar wave the scattered field about the target medium is measured.

Test #1. We have chosen two coaxial cylinders with $k = 10.1$, and $\tilde{\varepsilon}(\vec{x}) = \begin{cases} 0.02, \text{ for } 0.157 < \sqrt{(x_1^2 + x_2^2)} \leq 1.57 = \frac{\pi}{2}, \\ 0.006, \text{ for } \sqrt{(x_1^2 + x_2^2)} \leq 0.157 = 0.1\pi, \\ 0, \text{ otherwise.} \end{cases}$,

which describes a void located in the center having a radius 1/10th the radius of the outer cylinder. The relative errors for solution of the ISP obtained after different iterations are shown in Table 1. Note that in the first iteration we precisely invert the Born approximation. Therefore our method dramatically improves the accuracy of reconstruction compared to solutions limited to the Born approximation.

Table 1. Relative error %

Iteration	**1**	**2**	**3**	**4**	**5**	**6**	**7**	**9**	**10**	**11**	**12**
Error	**38**	**20**	**10.1**	**5.4**	**5.0**	**4.9**	**4.8**	**4.8**	**4.8**	**4.8**	**4.8**

Figure 4 represents the cross-section of these coaxial cylinders by a vertical plane through the origin. The dotted line represents the actual $\tilde{\varepsilon}(\vec{x})$ values and the solid line represents the computed values. To the best of our knowledge, this result is the first demonstration of recovery of an inclusion with an internal void.

In tests 2,3, and 5 we have used simulated data for different values of $\tilde{\varepsilon}(\vec{x})$. In tests 2 and 3 we have included 12 randomly distributed "spikes" which are in fact, cylinders of radius 0.02 and $\varepsilon = 0.008$. These we added to test how such data influences the computed results.

Test #2. Results in Figure 5 illustrate a complex sinusoidal void. We have assigned for $\vec{x} \in G$,

$\tilde{\varepsilon}(\vec{x}) = \begin{cases} 0.005, \text{ for } \sin(2x_1) - 0.9 < x_2 < \sin(2x_2), \\ 0, \text{ for } \frac{\pi}{2} < |x_1|, |x_2| < \pi, \\ 0.01, \text{ otherwise.} \end{cases}$ Figures 5a and 5b represent 3-D views of the actual and computed values of $\tilde{\varepsilon}(\vec{x})$; Figures 5c and 5d show top views of the same data without added spikes.

Test #3. Results in Figure 6 illustrate a medium with separate inclusions having complex geometry. For $\vec{x} \in G$ we have

assigned $\tilde{\varepsilon}(\vec{x}) = \begin{cases} 0.01, \text{ for } \sqrt{(x_1+0.2\pi)^2+(x_2+0.2\pi)^2} < 0.15\pi, \\ 0.01, \text{ for } 0.6 < x_1 < 1 \text{ and } 0.2 < x_2 < 1.3, \\ 0.01, \text{ for } 0.2 < x_1 < 1.3 \text{ and } 0.6 < x_2 < 1, \\ 0, \text{ otherwise.} \end{cases}$ Figures 6a and 6b represent 3-D views of the actual and computed $\tilde{\varepsilon}(\vec{x})$ values. Figures 6 c and d are top views of the same data. Results of the last two tests clearly demonstrate that our method is capable of resolving both the internal and external geometry of complex structures.

Test # 4. Results in Figure 7 illustrate a medium where we have included the smallest size of the cylinder which can still be seen by our method for N=10. We have chosen $\tilde{\varepsilon}(\vec{x}) = \begin{cases} 0.01, \text{ for } \sqrt{x^2{}_1+x^2{}_2} < 0.0314 = 0.01\pi, \\ 0, \text{ otherwise.} \end{cases}$ Figures 7a and 7b are representations of the Fourier series of N = 10 for the actual and computed functions in which the background value for ε is 1.4 rather than 1.0. Let A_1 be the area of this cylinder and A be the area of the cube G, then $A_1/A \approx 0.78 \times 10^{-4}$ which by eq. (1.4) is equivalent to having an added inclusion whose smallest diameter $r_s = .01\lambda$.

Test # 5. We have tested the resolution of our method at N=10. We have taken two cylinders of the radius r = 0.0314 and $\tilde{\varepsilon} = 0.01$, and $\tilde{\varepsilon} = 0$ otherwise. We have placed their centers in the points (a,0) and (-a, 0) and then moved these cylinders apart by changing a. We have discovered that the smallest value for a which can be resolved 0.24, and therefore the minimum distance between cylinders (i.e. distance between tangent lines, but not the centers) is 0.42. Thus, the dimensionless resolution R_S = 0.42 at N=10. Using rescaling, eq. (1.4), we conclude that R'_S = 0.13d in dimension variables. Figures 8a and 8b display the actual and computed values of $\tilde{\varepsilon}(\vec{x})$ for a = 0.24.

Test # 6. We have tested the stability of our method in terms of the effect that random noise in the data has on the resultant solution. Function $F(\vec{x},\vec{v})$ in (1.6) has been contaminated with a uniformly distributed random noise whose magnitude, P, varies from 10-200% of the maximum absolute value of function F. We have computed scattered field from a cylinder with $k = 5.3$ and $\tilde{\varepsilon}(x_1,x_2) = \begin{cases} 0.03, \text{ for } \sqrt{x_1{}^2+x_2{}^2} < 0.1, \\ 0, \text{ otherwise} \end{cases}$. The inverse problem was solved for N = 7. The relative error obtained after 12 iterations is shown in Table 2. Figure 9 illustrates a cross-section through the center of the actual, dotted line, and computed values, solid line, of the function $1+\tilde{\varepsilon}$ for P= 200%.

Table 2. Relative error (1.8) for different levels of noise/signal P

P, %	0	1	5	10	25	100	200
error%	4.33	4.36	4.68	5.45	9.97	33.2	68.9

Results for Time-Dependent Wave Equation

In our computational experiments we have solved the Field Extension problem, eqs. (2.13) by the Finite Element Method for a time-resolved signal. We started by choosing a value $w(\vec{x},t)$ such that w and $\frac{\partial w}{\partial n}$ vanish on $\partial D \times [0,T]$ and obtain

expressions for $f(\vec{x},t)$, that is $w_{tt}-\Delta w$ (see Fig. 2). Uniformly distributed random noise, of a magnitude σ was added to function f. That is we considered the function $f_\sigma(\vec{x},t)=f(\vec{x},t)(1+\sigma f)$, where σf is the random noise of magnitude σ, such that $|\sigma f|\le\sigma$. Thus, σ is equal to the noise/signal ratio. Then we computed function $u^\delta(\vec{x},t)$ for δ = 0.0001. Finally, we have calculated the relative error, $\dfrac{\|u^\delta-u\|}{\|u\|}$, where $\|\cdot\|$ is the $L_2(Q_T)$-norm (least squares norm). We have tested the following three functions

$$w_1=[1-\cos(2\pi x)][1-\cos(2\pi y)](t+1)^2,\quad f_1=w_{1tt}-\Delta w_1$$

$$w_2=100x^2(1-x)y^2(1-y)^2,\quad f_2=w_{2tt}-\Delta w_2$$

$$w_3=100x^2(1-x)^2y^2(1-y)^2e^{(x+y+t)},\quad f_3=w_{3tt}-\Delta w_3$$

Hence function w_3 changes very rapidly. In all our tests we have obtained approximately the same noise-relative error relations. These data are listed in Table 3.

Table 3. Relative Error for Solution of Field Extension Problem

Noise/signal ratio P, %	**0**	**5**	**10**
Relative error, %	**0.7**	**1.1**	**1.8**

Function $w_3(\vec{x},t)$ at t = 1.5 is presented in Fig. 10. Results in Table 3 show that the computed function w_3 is nearly identical to the function plotted in Figure 10.

4.0 Discussion

In this report we have described various strategies for solving the inverse scattering problem using time independent and time-resolved data, based on a wave optics approach, which is derived directly from the Maxwell's system. A goal in developing these schemes has been to identify a numerical treatment which is computationally efficient. Results presented here for the 2-D case confirm that the RQR method provides accurate reconstruction, in less than one minute of CPU time with a Y/MP-Cray processor, of media having complex internal structures. Because the strategies outlined here have been derived from fundamental relationships, these approaches should be capable of evaluating data obtained using electromagnetic and acoustic sources. Of particular interest is our demonstration that even when the acquired data are restricted to measuring the intensity of time-resolved signals, we are able to essentially recovery the "phase" data and compute solutions to the inverse problem. Recently, Klibanov et al. [20] have developed a version of the RQR approach for which the cost functional of the ISP for the time-resolved wave equation, with a single source location, is globally strictly convex. One advantage of this scheme is that, unlike the quasi-Newton method, it does not require any *a priori* estimate of the background properties of the target medium and, in principle, will converge to a single answer. It also differs from the quasi-Newton method in that it can provide solutions to the ISP using time-resolved data for media having a non-constant background. In the following we outline how the RQR scheme might be applied to evaluate time-resolved optical data obtained using ultrafast laser sources for highly scattering media.

It is well established that a traveling wave envelope can be represented in the form of $A\left(t-\dfrac{z}{v_g}\right)e^{i\omega\left(t-\frac{z}{v_g}\right)}$, where the real valued function A is the amplitude of the envelope traveling along the z axis in a nondispersive media before encountering the target medium, ϖ is the frequency of the carrier, v_g is the group velocity, and t is time. It can be shown from consideration of Maxwell's system that this equation describes the E_1 component of the electric field, $\vec{E}$, and $E_2 = E_3$

= 0. As mentioned previously, the same equation , with the same initial data, is also valid for the H_2 component of the magnetic field $\vec{H}$ and $H_1 = H_3 = 0$. This relationship is strictly valid in the case of a traveling wave where the derivative of function A is small compared to $\omega|A|$. Given that any real beam is restricted in the x-y directions, we should consider

$\frac{1}{\pi R^2}\exp\left[-\frac{x^2+y^2}{R^2}\right]A\left(t-\frac{z}{v_g}\right)e^{i\omega\left(t-\frac{z}{v_g}\right)}$, where we introduce the Gaussian function $\frac{1}{\pi R^2}\exp\left[-\frac{x^2+y^2}{R^2}\right]$ and R is equivalent to the width of the pulse with respect to x,y. When $R \to 0$, we obtain $\delta(x,y)A\left(t-\frac{z}{v_g}\right)e^{i\omega\left(t-\frac{z}{v_g}\right)}$. By rescaling the time and z-axis such that the Gaussian beam shape, A, approximates a delta function, we obtain Cauchy initial data as described in equation 2.1. As is was shown, E_1 and H_2 satisfy the same wave equation with the same initial data such that $E_1(\vec{x},t) \equiv H_2(\vec{x},t)$, for $t > 0$. It follows that the length of the Pointing vector equals the measured intensity, $I = E_1^2 = H_2^2 = u^2$, where function u was introduced earlier, and is equivalent to equation 2.4. As mentioned above the function u equals $\pm\sqrt{I}$. However it is evident from inspection of any temporal profile that the measured intensity is always a positive number [25]. Thus we can consider the relationship $u = +\sqrt{I}$. Input data for the inverse problem described by equation (2.5) is therefore obtained by simply computing the square-root of the measured intensity of the temporal profile at all time points. These considerations would indicate, therefore, that the numerical treatments described here may be applicable for evaluating time-resolved optical data from dense scattering media (e.g. tissues) obtained using ultra-fast laser sources.

It is interesting to note that the above suggestion regarding evaluation of optical data obtained from highly scattering media using wave-optic approaches, would appear consistent with recent numerical and experimental results by Sevick et al [30] and Gratton et al. [31], who have provided convincing arguments of the existence of wave-like phenomenon propagating in dense scattering media. These so-called photon-density waves can be observed by directing an amplitude modulate laser source to a scattering medium [32]. Furthermore, it has been demonstrated that, in homogeneous scattering media, these waves will propagate at constant velocity, undergo refraction and reflection at boundaries [33], and when produced using sources having appropriate phase delays will generate a null plane entirely similar to well established methods used in phased array radar imaging [34]. It has also been correctly pointed out that measurements performed in the frequency domain, in principle, contain the same information provided by time-resolved data, as the two are related by being a Fourier pair. As a point of clarification, however, it deserves mention that whereas the results from this operation will be related to the Fourier transform performed in eq. (2.6), they are *not* equivalent, as this operation is performed on $\sqrt{I}$ rather than I.

As mentioned in the Introduction, interest in the possibility of generating 3-D images of tissue based on NIR optical measurements has recently received considerable attention. Currently, several teams, including some of the co-authors are pursuing image recovery schemes based on a particle formulation. A linear perturbation model derived from the transport equation for solution to the 3-D inverse problem was first introduced by Barbour et al. in 1988 [35, 36]. An important feature of this approach is the ability to explicitly relate the response of detectors located at the surface to non-linear spatial volume functions which identify the site dependent effect of absorption and scattering inside the medium [37]. The formulation is completely general and, in principle, can consider any arbitrarily shaped medium having arbitrary internal structure. While originally formulated to consider time-independent measurements [38], this scheme has been extended to include measurements performed in the time- and frequency-domain [39], and is capable of yielding 3-D images of the absorption, scattering and fluorescence properties of highly scattering media such as body tissues [39]. Recently, Graber et al. [39,40] have experimentally validated this scheme for simply structured media based on time-independent absorption measurements performed at 720 nm evaluated using one-step of the perturbation equation. The target medium consisted of a 2% suspension of Intralipid® (1:5 dilution of 10% stock solution), which has an optical

thickness roughly equivalent to a uncompressed female breast. Included in this medium was a single object (i.e. a glass rod filled with diluted ink) whose cross-sectional area was 0.34% the area of the vessel, and the computed 3-D image demonstrated an resolution of edge of 0.8 mm.

A method similar to the perturbation model described above, but based on solutions to the diffusion equation, has been described by Arridge et al. [8]. An important aspect of their work has been the emphasis placed on employing regularization methods. These authors have also described formulations which can evaluate, simultaneously, the absorption and scattering properties of the target medium [8]. A method capable of providing a similar determination has been described by Grunbaum et al [9] based on a discretization of the transport equation in the spatial and angular domains. The method is applicable to arbitrarily shaped objects and involves iterative solutions of the forward and inverse problem. An iterative discrete particle based scheme has also been proposed by Schlereth et al [41] and is cast as a learning problem in a neural net structure. This approach is appealing as it should be capable of incorporating information derived from both wave-optic and particle formations of the ISP.

Regardless of which approach or combination of approaches ultimately proves most successful for solving the optical ISP, it is very clear that the acquisition of high quality data will be an important factor. A basic advantage of time resolved measurements is that it directly yields information regarding the probability of photon exit as a function pathlength and therefore time. To the extent that an unscattered, or ballistic component, can be readily measured, then procedures applicable to CT imaging (i.e. Radon transform) would apply. However, for most applications of practical interest, it seems unlikely that this signal will either not exit or have a poor signal to noise ratio. A more useful quantity to evaluate might be to consider photons which exit the medium at times slightly longer than the theoretical minimum. These have been referred to previously as "snake photons" [25] and given that the standard deviation of the spatial distribution of paths is less than for photons exiting at latter times [42], it can be expected that the precision of measurement corresponding to these early photons will be greater compared to photons exiting at later times. This observation is, in fact, well known [43]. Additionally, because the degree of scattering experienced by these photons is less, the uncertainty associated concerning the paths of the detected photons will also be less. Assuming that the derivation outlined above holds in practice, the RQR scheme described provides at least two approaches to make use of this information to provide for solution of the optical ISP.

In one case, we could consider use of the field extension problem, in combination with the quasi-Newton method for the time-resolved wave equation. The latter can directly evaluate the ISP (2.9), (2.10), using equations (2.11) and (2.12) which make use of only the early arriving light. This approach assumes a priori knowledge of the background properties of the target medium and that these values are quasi-constant. An attractive aspect of this scheme is that the computation of the time-resolved response about some sub-volume of interest readily lends itself to experimental verification by placement of optical fibers within the medium.

In a second case, we could employ globally strictly convex minimizing cost functionals. While this approach does not require explicit knowledge of the background properties of the target medium it does consider a reference medium against which measured responses are compared. Clearly, because the standard deviation of the spatial volume function declines at early times, use of earlier, as opposed to later, arriving photons will increasingly interact with a given specified volume, thereby providing more reliable information.

Practical solution of the ISP's of the types examined here represent a difficult but solvable problem. As emphasized above, the size of the computations encountered are usually very large, especially for the 3-D case. Recent development of low cost parallel computing systems offer the promise, however, of providing the needed computation speed which should serve to accelerate development of more efficient and stable inversion schemes. While the practical development of optical imaging schemes is by no means assured, considerations of the favorable cost, sensitivity, and temporal resolution together with other factors would suggest that continued efforts in this area should proceed briskly for the foreseeable future.

5.0 References

[1] P. L. Nunez, "High resolution EEG: applications in medicine and cognitive science", accompanying paper in these proceedings, 1993.

[2] Z. L. Lu, "Magnetic Source Imaging of the Human Brain", accompanying paper in these proceedings, 1993.

[3] M. Cheney, and D. Isaacson, "Imaging the interior of the body with electric fields", accompanying paper in these proceedings, 1993.

[4] C. L. Dumoulin, M. Tarnawski, D. J. Doorly, C. G. Caro, and R. D. Darrow, "Measurement of physiological flow parameters with magnetic resonance", accompanying paper in these proceedings, 1993.

[5] D. Le Bihan, C. A. Cuenod, R. Turner, P. Jezzard, V. Bonnerot and T. Zeffiro, "Functional imaging of the brain by MRI", accompanying paper in these proceedings, 1993.

[6] D. L. Colton, and P. V. Monk, "The inverse scattering problem for time-harmonic acoustic waves in an inhomogeneous medium: numerical experiments", IMA J. Appl. Math., 42, 77-95, 1989.

[7] R. L. Barbour, H. L. Graber, Y. Wang, J. Chang, and R. Aronson, "A perturbation approach for optical diffusion tomography using a continuous-wave and time-resolved data", Proceedings SPIE Institute on Medical Optical Tomography, 1993, in press.

[8] S. R. Arridge, M. Schweiger, and D. T. Delpy, " Iterative reconstruction of near infra-red absorption images" in SPIE vol. 1767, Inverse Problems in Scattering and Imaging, 372-383, 1992

[9] F. A. Grunbaum and J. P. Zubelli, "Diffuse Tomography" accompanying paper in these proceedings, 1993.

[10] W. F. Chenong, S. A. Prahl, and A. J. Welch, "A review of the optical properties of biological tissues", IEEE J. Quantum Elec. vol, 26, 2166-2185, 1990.

[11] A. C. Kak and M. Slaney, Principles of Computerized Tomographic Imaging, IEEE Press, chapter 6, pp 203-274, 1988.

[12] Y. M. Wang and W. C. Chew, "An iterative solution of the two-dimensional electromagnetic inverse scattering problem", Int. J. of Imaging Systems and Technology, vol. 1, 100-108, 1989.

[13] W. C. Chew and Y. M. Wang, "Reconstructions of two-dimensional permittivity distribution using the distorted Born iterative method", IEEE Trans. Med. Imag., vol., 2, 218-225, 1990.

[14] D. Colton and P. Monk, "The numerical solution of an inverse scattering problem for acoustic waves", IMA J. Appl. Math., vol. 49, pp. 163-184, 1992.

[15] D. Colton and P. Kress, Inverse Acoustics and Electromagnetic Scattering Theory, Appl. Math. Sci., vol. 93, Springer Verlag, New York, 1992.

[16] R. E. Kleinman and P. M. van den Berg, "Nonlinearized approach to profile inversion", Int. I Imag. Syst. Tech., vol 2, pp 119-126, 1990.

[17] P. C. Sabatier, ed., "Modeling or solving inverse problems", in Inverse Methods in Action, Springer-Verlag, New York, pp. 1-14, 1990.

[18] M. V. Klibanov, S. Gutman and O.V. Ioussoupova, "Multi-dimensional inverse scattering problems in random and deterministic media," Proc. SIAM Conf. of Wave Propagation Phenomenon, 1993.

[19] S. Gutman and M. V. Klibanov, "Regularized quasi-Newton method for inverse scattering problems", Int. J. Math. Comp. Modeling, 1993.

[20] M. V. Klibanov, and O. V. Ioussoupova, "Uniform strict convexity of a cost functional for 3-D inverse scattering problem", submitted, SIAM, J. Math. Analysis, 1993.

[21] M. V. Klibanov and J. Malinsky, "Newton-Kantorovich method for 3-dimensional potential inverse scattering problem with time dependent data", Inverse Problems, vol. 7, pp 577-596, 1991.

[22] M .V. Klibanov and Rakesh, "Numerical solution of a time-like Cauchy problem for the wave equation", Math. Methods in Appl. Sci., vol., 15, pp 559-570, 1992.

[23] J. D. Jackson, Classical Electrodynamics, John Wiley and Sons, New York, 1977.

[24] S. R. Chandraseckar, Radiative Transfer, Oxford, 1950.

[25] K. M. Yoo, B. B. Das, and R. R. Alfano, "Imaging of translucent object hidden in a highly scattering medium from the early portion of the diffusive component of a transmitted ultrafast laser pulse", Opt. Lett., vol. 17, pp. 958-960, 1992.

[26] M. M. Lavrent'ev, V. G. Romanrov and A. P. Shishatskii, Ill-Posed Problems of Mathematical Physics and Analysis, vol. 64, Amer. Math. Society, Providence, RI. , 1986.

[27] M. V. Klibanov, "Inverse problems and Carleman estimates", Inverse Problems, vol. 8, pp 575-596, 1992.

[28] P. Colli-Franzone, S. Tentone, C. Viganotti, S. Bacriffi, S. Spaggiari and B. Taccardi, "A mathematical procedure for solving the inverse potential problem of electrocardiography for in vitro experimental data", Math. Biosci., vol. 77, 1985, pp 353-396.

[29] C. R. Johnson, and R. S. Macleod, "Computational studies of forward and inverse problems in electrocardiography", in Biomedical Modeling and Simulations, J. Eisenfeld, M. Witten and D. S. Levine, eds., Elsevier, Amsterdam, pp 283-290, 1992.

[30] E. M. Sevick, B. Chance, J. Leigh, S. Nioka and M. Maris, "Quantitation of time- and frequency-resolved optical spectra for the determination of tissue oxygenation", Anal. Biochem. 195, 330-351 (1991).

[31] J. B. Fishkin, E. Gratton, M. J. vandeVen, W. W. Mantulin, "Diffusion of Intensity Modulated Near-Infrared Light in Turbid Media." SPIE vol. 1431, 122-135., 1991.

[32] J. B. Fishkin and E. Gratton, "Propagation of photon-density waves in strongly scattering media containing an absorbing semi-infinite plane bounded by a straight edge" J. Am. Soc. Am. vol. 10, 127-140, 1993.

[33] M. A. O'Leary, D. A. Boas, B. Chance, and A. G. Yodh "Refraction of Diffuse Photon Density Waves", Phys. Rev. Lett. 69, 2658-2661, 1992.

[34] B. Chance, "Inphase-Antiphase Multi-Element Array", SPIE vol. 1888, in Photon Migration and Imaging in Random Media and Tissues, 1993, in press.

[35] R. L. Barbour, J. Lubowsky, and H. Graber, "Use of reflectance spectrophotometry as a possible 3-dimensional spectroscopic imaging technique" FASEB J. vol 2, a1772, 1988.

[36] R. L. Barbour, J. Lubowsky and R. Aronson, "Method of imaging a random medium" US Patent no. 5,137,355, (filed June 8, 1988, issued Aug. 11, 1992).

[37] R. L. Barbour, H. Graber, R. Aronson and J. Lubowsky, "Model for 3-D optical imaging of tissue" Proc. 10th annual Int. Geosci. and Remote Sensing Symposium, (IGARSS) Vol II, pp. 1395-1399, 1990.

[38] R. L. Barbour, H. L. Graber, R. Aronson and J. Lubowsky, "Imaging of subsurface regions of random media by remote sensing" SPIE vol. 1431, 192-203., 1991.

[39] H. L. Graber, J. Chang, R. Aronson and R. L. Barbour, "A perturbation model for imaging in dense scattering media: Derivation and evaluation of imaging operators," Proceedings SPIE Institute on Medical Optical Tomography, 1993, in press.

[40] H. L. Graber, J. Chang, J. Lubowsky, R. Aronson and R. L. Barbour, "Near infrared absorption imaging of dense scattering media by steady-state diffusion tomography," SPIE vol. 1888, in Photon Migration and Imaging in Random Media and Tissues, 1993, in press.

[41] F. H. Schlereth, J. M. Fossaceca, A. D. Keckler and R. L. Barbour, "Imaging in diffusing media with a neural net formulation: A problem in large scale computation," SPIE vol. 1641, Physiological Monitoring and Early Detection Diagnostic Methods, pp. 46-57, 1992.

[42] R. L. Barbour, H. L. Graber, J. Lubowsky, R. Aronson, B. B. Das, K. M. Yoo, R. R. Alfano, "Imaging of diffusing media by a progressive iterative backprojection method using time-domain data", SPIE vol. 1641, ibid. pp. 21-34, 1992.

[43] K. M. Yoo, and R. R. Alfano, "Time-resolved coherent and in-coherent components of forward light scattering in random media", Opt. Lett. vol. 15, pp 320-322, 1990.

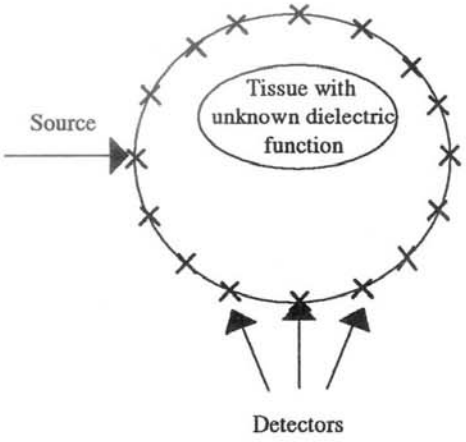

Figure 1. Schematic of measurement scheme

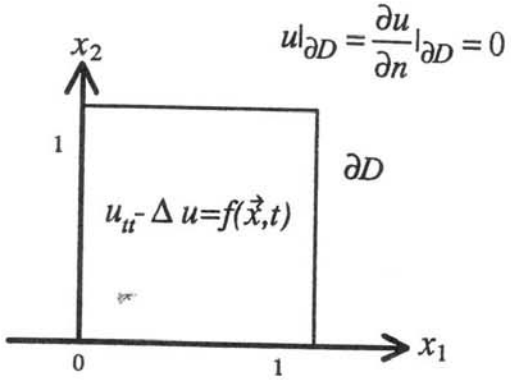

Figure 2. Field Extension Problem

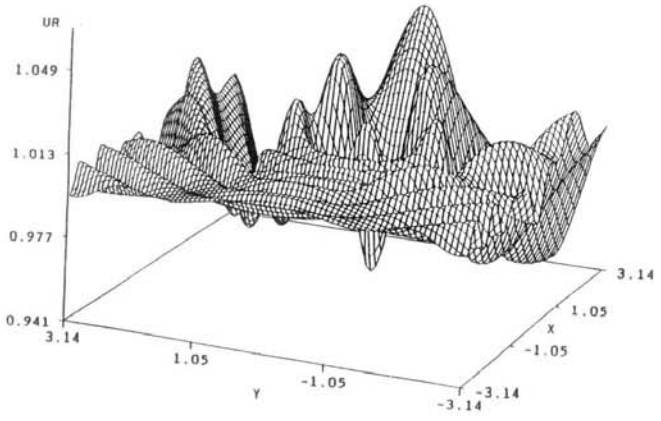

Figure 3

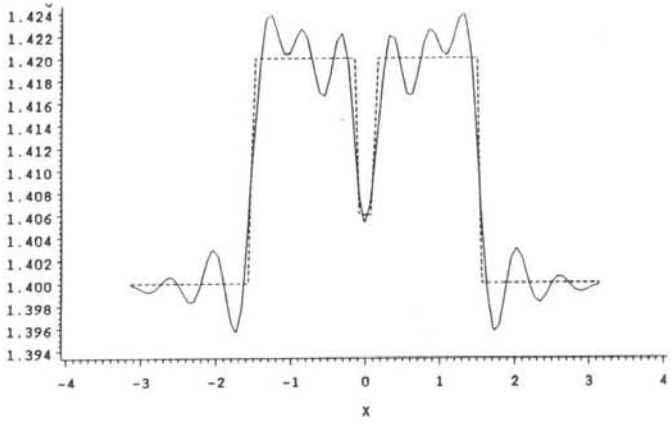

Figure 4

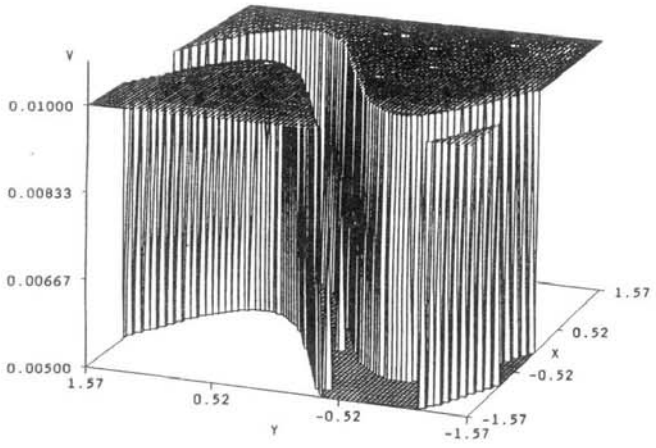

Figure 5a

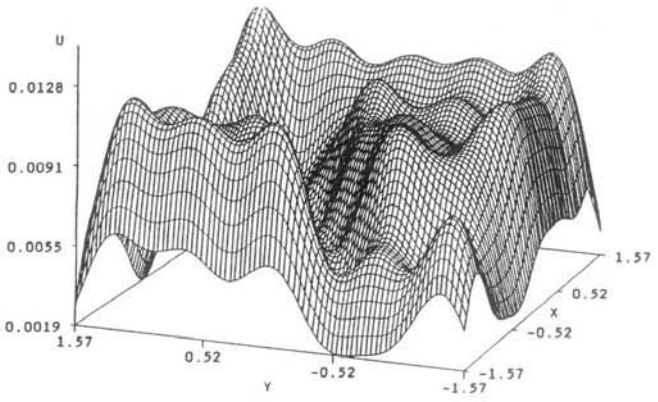

Figure 5b

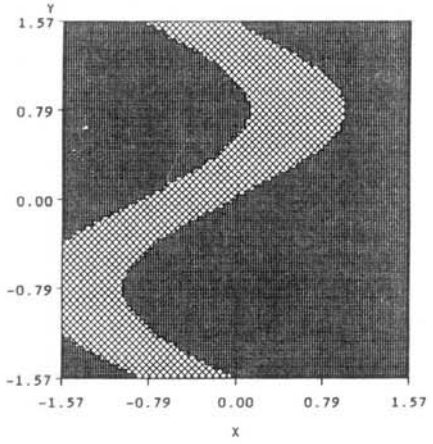

Figure 5c

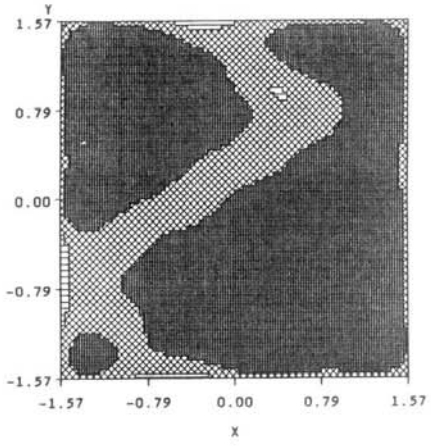

Figure 5d

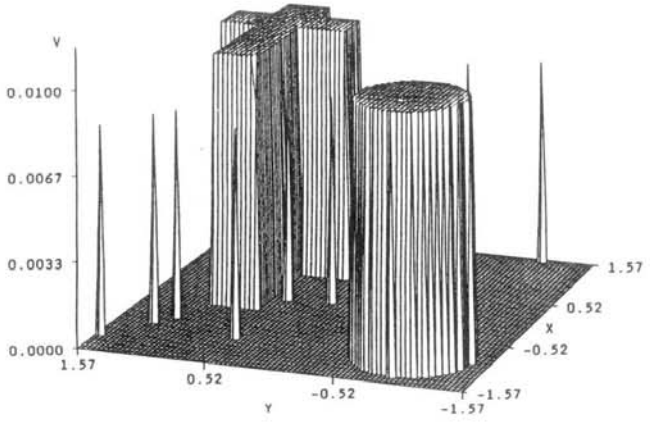

Figure 6a

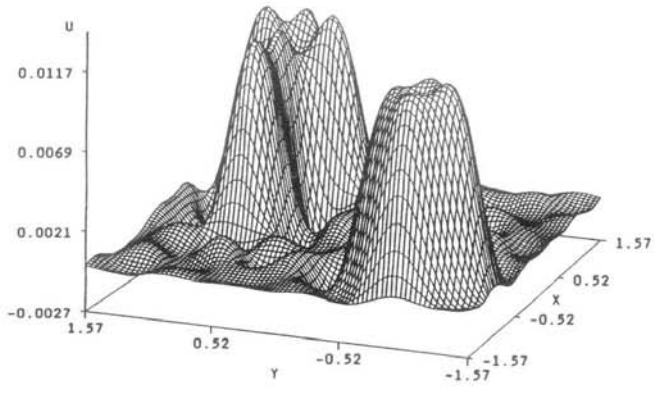

Figure 6b

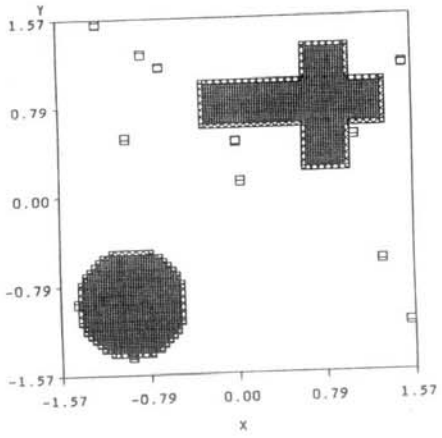

Figure 6c

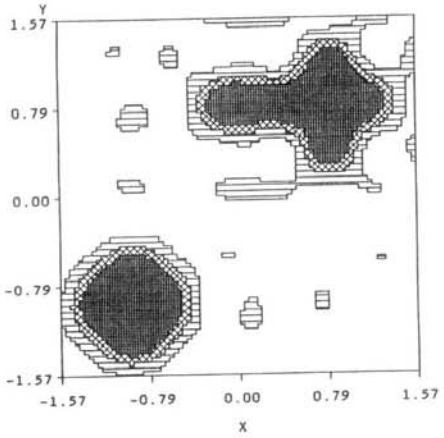

Figure 6d

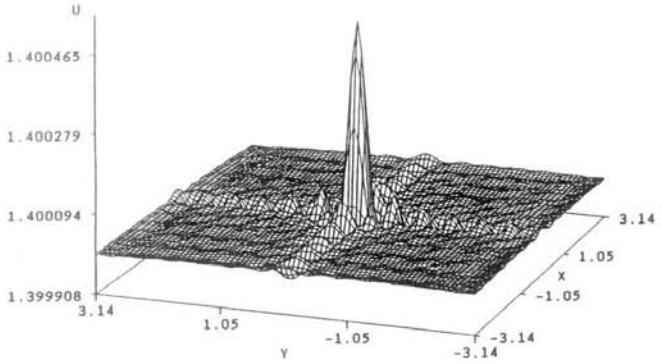

Figure 7a

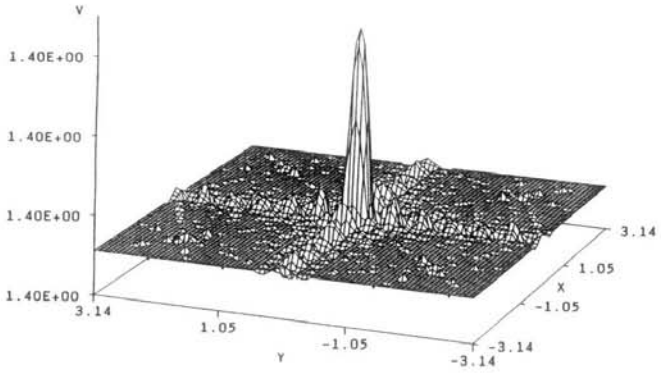

Figure 7b

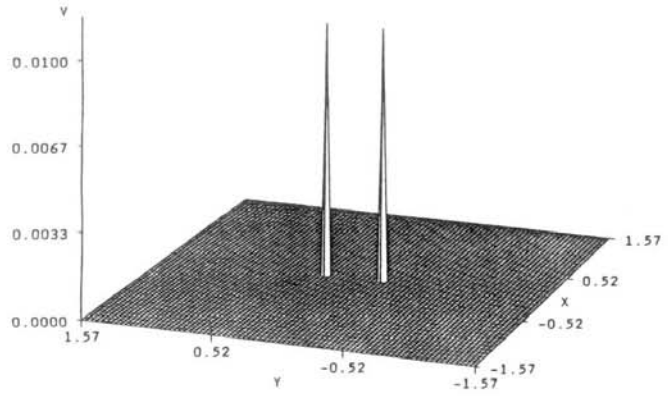

Figure 8a

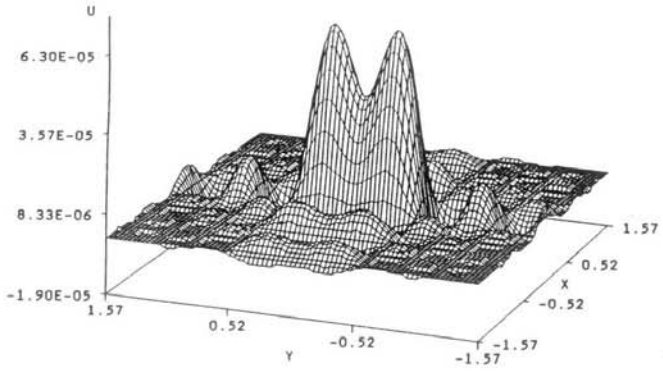

Figure 8b

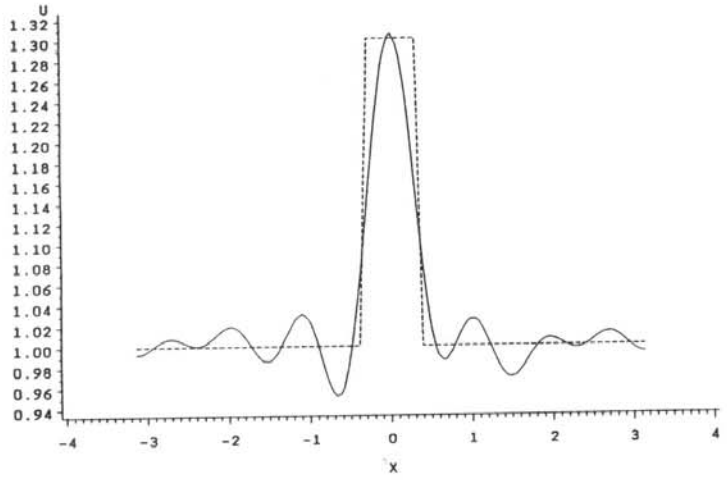

Figure 9

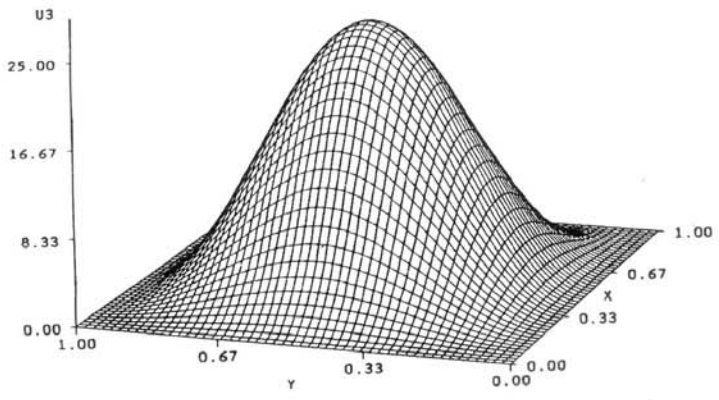

Figure 10